Earth's Future

RESEARCH ARTICLE
10.1029/2021EF002141

Heavy Precipitation Impacts on Nitrogen Loading to the Gulf of Mexico in the 21st Century: Model Projections Under Future Climate Scenarios

Jien Zhang[1], Chaoqun Lu[1], William Crumpton[1], Christopher Jones[2], Hanqin Tian[3], Gabriele Villarini[2], Keith Schilling[4], and David Green[1]

[1]Department of Ecology, Evolution, and Organismal Biology, Iowa State University, Ames, IA, USA, [2]IIHR—Hydroscience & Engineering, University of Iowa, Iowa City, IA, USA, [3]School of Forestry and Wildlife Sciences, International Center for Climate and Global Change Research, Auburn University, Auburn, AL, USA, [4]Iowa Geological Survey, Iowa City, IA, USA

Abstract While spatial heterogeneity of riverine nitrogen (N) loading is predominantly driven by the magnitude of basin-wide anthropogenic N input, the temporal dynamics of N loading are closely related to the amount and timing of precipitation. However, existing studies do not disentangle the contributions of heavy precipitation versus non-heavy precipitation predicted by future climate scenarios. Here, we explore the potential responses of N loading from the Mississippi Atchafalaya River Basin to precipitation changes using a well-calibrated hydro-ecological model and Coupled Model Intercomparison Project Phase 5 climate projections under two representative concentration pathway (RCP) scenarios. With present agricultural production and management practices, N loading could increase up to 30% by the end of the 21st century under future climate scenarios, half of which would be driven by heavy precipitation. Particularly, the RCP8.5 scenario, in which heavy precipitation and drought events become more frequent, would increase N loading disproportionately to projected increases in river discharge. N loading in spring would contribute 41% and 51% of annual N loading increase under the RCP4.5 and RCP8.5 scenarios, respectively, most of which is related to higher N yield due to increases in heavy precipitation. Anthropogenic N inputs would be increasingly susceptible to leaching loss in the Midwest and the Mississippi Alluvial Plain regions. Our results imply that future climate change alone, including more frequent and intense precipitation extremes, would increase N loading and intensify the eutrophication of the Gulf of Mexico over this coming century. More effective nutrient management interventions are needed to reverse this trend.

Plain Language Summary Future climate change is expected to alter nutrient transport from land to rivers, which will have impacts on coastal ecosystems. The impacts of future precipitation changes on nitrogen (N) loading, however, remain unclear. Based upon a well-tested hydro-ecological model, this study separates the roles of future heavy precipitation, non-heavy precipitation, and no-precipitation days in affecting N leaching loss and predicts the changes in N loading to the Gulf of Mexico. N loading is projected to increase by 30% under two climate scenarios (RCP4.5 and RCP8.5) by the end of the 21st century, half of which is likely driven by heavy precipitation. Future increases in spring heavy precipitation likely result in higher N leaching loss and enhance N loading. Our results indicate that more effective nutrient reduction efforts will be needed to reach the reduction goals of N loading and hypoxia extent in the Gulf of Mexico.

Key Points:

- We examine the responses of nitrogen (N) loading from the Mississippi Atchafalaya River Basin (MARB) to future climate changes
- N loading from the MARB could increase by 30% under future climate scenarios, and half of the increase would be driven by heavy precipitation
- Anthropogenic N input would be increasingly susceptible to leaching loss in the Midwest and Mississippi Alluvial Plain under future climate

Supporting Information:

Supporting Information may be found in the online version of this article.

Correspondence to:

C. Lu,
clu@iastate.edu

Citation:

Zhang, J., Lu, C., Crumpton, W., Jones, C., Tian, H., Villarini, G., et al. (2022). Heavy precipitation impacts on nitrogen loading to the Gulf of Mexico in the 21st century: Model projections under future climate scenarios. *Earth's Future*, *10*, e2021EF002141. https://doi.org/10.1029/2021EF002141

Received 7 APR 2021
Accepted 14 MAR 2022

Author Contributions:

Conceptualization: Jien Zhang, Chaoqun Lu
Data curation: Jien Zhang
Formal analysis: Jien Zhang, Chaoqun Lu
Funding acquisition: Chaoqun Lu
Investigation: William Crumpton, Christopher Jones, Hanqin Tian, Gabriele Villarini, Keith Schilling, David Green

1. Introduction

Increasing nutrient pollution in water bodies has become a global concern (Sinha et al., 2017). Excessive agricultural nitrogen (N) leached from soils and transported through river channels is a major driver of the formation and extent of hypoxic zones and algal blooms in estuaries and coastal waters (Howarth et al., 2000; Howarth & Marino, 2006). Since the 1960s, synthetic N fertilizer use has increased ninefold globally (Lu & Tian, 2017), resulting in widely documented degradation of water quality (Evans et al., 2012; Grizzetti et al., 2011; Rabalais et al., 2007). Climate change is expected to increase the riverine N loading in many regions around the world (Howarth et al., 2006). Human-induced climate change has influenced the occurrence and the magnitude of extreme climatic events (National Academies of Sciences, Engineering, and Medicine, 2016). Therefore, understanding the response of land-to-aquatic N loading to extreme climatic events is urgent and critical for better N management and the assessment of progress toward reducing riverine N loading. Although previous studies

Project Administration: Chaoqun Lu
Supervision: Chaoqun Lu
Validation: Jien Zhang
Writing – original draft: Jien Zhang
Writing – review & editing: Jien Zhang, Chaoqun Lu, William Crumpton, Christopher Jones, Hanqin Tian, Gabriele Villarini, Keith Schilling, David Green

have demonstrated the impacts of historical precipitation events on riverine N loading (Lu et al., 2020; Sinha et al., 2017; Tian et al., 2020), it remains unclear how future changes in the intensity and timing of precipitation events will affect riverine N loading.

Previous study has shown that year-to-year variations in precipitation amount drive over three-quarters of the interannual variability of N loading, and extreme precipitation events have been reported to only slightly influence N loading variations (Ballard et al., 2019; Donner & Kucharik, 2003; Sinha et al., 2017; Sinha & Michalak, 2016). However, other research shows that heavy precipitation could play an important role in enhancing nutrient loading under both historical and projected climate change conditions across scales (Carpenter et al., 2018; Zheng et al., 2020). Particularly, heavy rainfall after multiyear dry spells could potentially increase N loading in the Susquehanna River Basin by 40%–65%, leading to enlarged hypoxic zones (Lee et al., 2016). Such a debate on the heavy precipitation impacts on N loading arises primarily for two reasons: (a) existing research solely focused on the changes in annual or monthly precipitation (Ballard et al., 2019; Sinha & Michalak, 2016), which did not quantify the contributions of precipitations with different intensities (e.g., heavy precipitation vs. non-heavy precipitation) on N loading at a daily time step, and (b) re-assembled natural climate variability and continuity were used to force factorial modeling experiments (Lee et al., 2016), which did not necessarily reflect the real-world spatiotemporal changes in N loading. These methodological limitations raise the concern that future N loading will be difficult to predict without fully considering the various impacts of heavy and non-heavy precipitation in the coming decades.

Nutrient discharge from the Mississippi Atchafalaya River Basin (MARB) in the United States forms the world's second-largest hypoxic zone in the receiving Gulf of Mexico (Thomas & Rahman, 2012). A previous study has shown that the MARB will likely experience large increases in heavy precipitation in the coming century (Janssen et al., 2016). Here, we quantify the impacts of future precipitation events (e.g., rain and snow) with different intensities on riverine N loading across the MARB using a daily time-step process-based hydro-ecological model, the Dynamic Land Ecosystem Model (DLEM). The DLEM model considers the short-term and long-term legacy effects of precipitation on changes in water and N yield (Lu et al., 2020; Tian et al., 2020). In DLEM, snowfall does not directly induce N leaching or loading but can affect soil moisture in early spring due to snow melting, altering water yield (i.e., surface and subsurface runoff) as well as N yield. Such processes may not be triggered until the snow starts melting in DLEM. This delayed effect will apply to the extreme snowfall as well. The goals of this study are to (a) examine the patterns of future heavy precipitation (HP, daily precipitation is over the monthly 90th percentiles) across the MARB under two climate scenarios (i.e., two representative concentration pathways [RCPs] scenarios, namely RCP4.5 and RCP8.5 as known as a "medium stabilization scenario" and a " high baseline emission scenario", respectively, based on greenhouse gas concentration trajectories; Figure 1), (b) estimate the contributions of annual total precipitation (TP), HP events, non-HP events, and no-precipitation days to water yield and N yield across the MARB by the end of the century, and (c) identify the spatial hotspots of increases in water yield and N yield driven by precipitation intensity change. We use the climate projections generated by three Coupled Model Intercomparison Project 5 (CMIP5) models to force a hydro-ecological model, DLEM, that incorporates land hydrological and biogeochemical processes with a networked river system. Over the study period, the MARB exhibits no significant trends in annual precipitation under future climate scenarios. This near-stationarity in annual precipitation exposes the role of daily variations of precipitation intensity in driving N loading. Our analysis shows that HP is strongly associated with increases in water and N yield by the end of the century.

2. Methods

2.1. Data Sources

We obtain the future (defined as 2018–2099) daily climate data (temperature, precipitation, and shortwave radiation) from the Multivariate Adapted Constructed Analogs (MACA)v2-METDATA data set (http://www.climatologylab.org/maca.html) that is at 4 × 4 km^2 resolution for the United States. They are generated by three CMIP5 Earth System Models (ESMs) for the RCP4.5 and RCP8.5 scenarios (Table 1). Among the three ESMs, the HadGEM2-ES and the GFDL-ESM2G respectively represent the high and low bound of the projected global climate warming in the 21st century (Figure 1a), and the CNRM-CM5 is representative of the mid-values of equilibrium climate sensitivity in the CMIP5 suite. The climate data are resampled to 5-arc min resolution using the inverse distance weighted interpolation to match the resolution of other input drivers used in this study. The

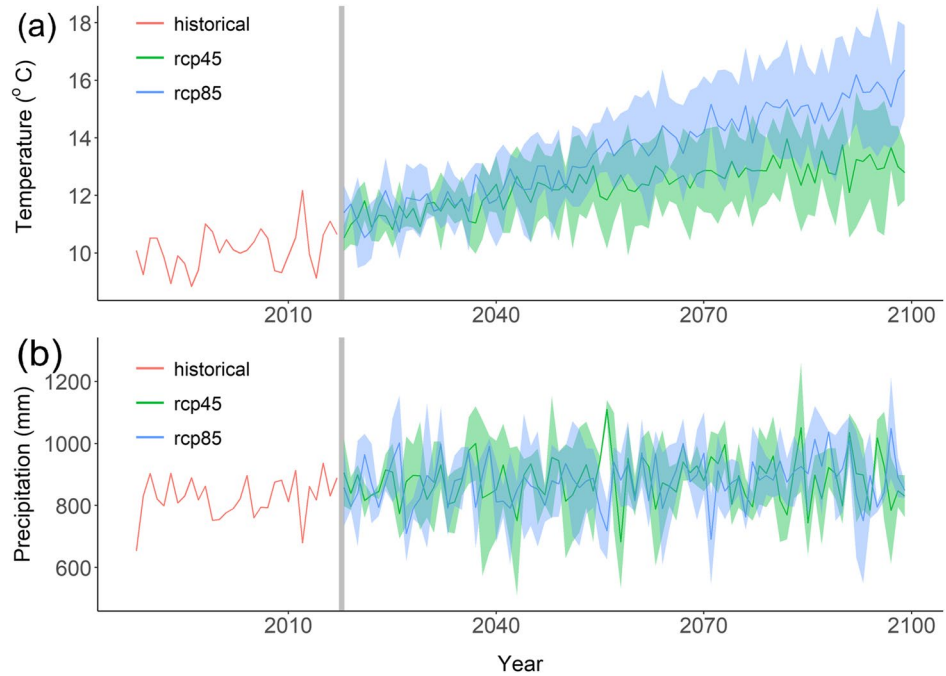

Figure 1. Mean annual temperature (a) and annual total precipitation (b) in the MARB for the historical period (1988–2017) from instrumental measurements by the METDATA climate data (Abatzoglou, 2013) and future period (2018–2099) projected by the three Coupled Model Intercomparison Project 5 (CMIP5) climate models. The shaded area in (a) and (b) indicates the standard deviation across the three CMIP5 models. The red curves indicate the historical period from 1988 to 2017.

historical climate data from 1979 to 2017 are downloaded from the MACA Training Data (https://climate.northwestknowledge.net/MACA/MACAtrainingdata.php). These training climate data, which are used to bias-correct and downscale the CMIP5 climate data in both the historical and future periods, are from the observation-based METDATA climate data developed by Abatzoglou (2013). The MACA downscaling method exhibits well performance in temperature, humidity, wind, and precipitation due to its ability to jointly downscale temperature and dew point temperature and its use of analog patterns rather than interpolation (Abatzoglou & Brown, 2012). For the period from 1901 to 1978, we use the CRU-NARR climate data (Mesinger et al., 2006; Mitchell & Jones, 2005) to drive our model in the way as our previous studies (Lu et al., 2018, 2020; Yu et al., 2018). To develop a spatiotemporally consistent climate data set, we adjust the CRU-NARR climate data based on the MACA historical training data, namely the METDATA, by using a revised delta method (Liu et al., 2013). We first calculate a long-term average annual temperature and monthly temperature from 11 overlapping years (1979–1989) for the two climate data sources. The ratio of monthly temperature range between the two datasets is calculated as:

$$R = \left(T^{max}_{MACA-train} - T^{min}_{MACA-train}\right) / \left(T^{max}_{CRU-NARR} - T^{min}_{CRU-NARR}\right) \quad (1)$$

where $T^{max}_{MACA-train}$ and $T^{min}_{MACA-train}$ are the maximum and minimum monthly temperatures from the MACA historical training climate data; $T^{max}_{CRU-NARR}$ and $T^{min}_{CRU-NARR}$ are the maximum and minimum monthly temperatures

Table 1
CMIP5 Models Used for the Simulations

Model name	Original resolution	Adjusted resolution	Model country	Historical period	Future period	References
CNRM-CM5	1.4° × 1.4°	0.083° × 0.083°	France	1961–2017	2018–2099	Voldoire et al. (2013)
GFDL-ESM2G	2.5° × 2.0°	0.083° × 0.083°	USA	1961–2017	2018–2099	Dunne et al. (2013)
HadGEM2-ES	1.88° × 1.25°	0.083° × 0.083°	UK	1961–2017	2018–2099	Collins et al. (2011)

from the CRU-NARR data from 1979 to 1989, respectively. Then we calculate the difference between the MACA annual temperature and the adjusted CRU-NARR annual temperature:

$$\Delta T = T_{CRU-NARR} \times R - T_{MACA-train} \quad (2)$$

where $T_{CRU-NARR}$ is the 11-year annual average temperature of the CRU-NARR data, R is the above-estimated ratio, and $T_{MACA-train}$ is the 11-year annual average temperature of the MACA-training data. The daily CRU-NARR temperature data from 1901 to 1978 are then adjusted as:

$$T_{adj,d} = T_d \times R - \Delta T \quad (3)$$

where T_d is the original CRU-NARR daily temperature, and $T_{adj,d}$ is the adjusted daily temperature that is used to drive simulations in this study. Through this modification, we not only modify the magnitude of CRU-NARR temperature but also reserve the annual amplitude signal from the MACA training data. The adjustment of radiation data is the same as the temperature data. Because the precipitation data is not continuous, we adjust the precipitation by using the ratio (R') of annual average precipitation between the two data sources:

$$R' = \left(P^{sum}_{MACA-train} / P^{sum}_{CRU-NARR}\right) \quad (4)$$

where $P^{sum}_{MACA-train}$ and $P^{sum}_{CRU-NARR}$ are the annual average precipitation from 1979 to 1989 from the MACA-training data and the CRU-NARR data, respectively.

$$P_{adj,d} = P_d \times R' \quad (5)$$

where P_d is the original CRU-NARR daily precipitation, $P_{adj,d}$ is the adjusted CRU-NARR daily precipitation, and R' is the ratio of the annual total precipitation averaged from 1979 to 1989 calculated between the two climate data sources.

Atmospheric CO_2 concentration for the 21st century is retrieved from the RCP Database (version 2.0) for the two examined scenarios (Clarke et al., 2007; Riahi et al., 2007; Smith & Wigley, 2006; Wise et al., 2009). Specifically, the RCP4.5 scenario represents the radiative forcing level stabilizes at 4.5 W m^{-2} before 2100 by utilizing a range of technologies and strategies for reducing greenhouse gas emissions (Thomson et al., 2011), and the RCP8.5 scenario stands for the radiative forcing level at 8.5 W m^{-2} characterized by high greenhouse gas concentration levels over time (Riahi et al., 2011).

The historical spatial N deposition data are obtained from the National Atmospheric Deposition Program (NADP) for the period 2000–2017 and extended to the period before 2000 by following the trend of global gridded N deposition data (Dentener, 2006; Wei et al., 2014). The time-series gridded data of historical crop-specific N fertilizer use rate, timing, and types used in this study are from Cao et al. (2018). Historical land use and land cover change data used in this study are from Yu and Lu (2018), which includes time-varying gridded maps of crop types from 1850 to 2016. The dynamic extent of cropland distribution and interannual crop rotations are incorporated in our simulations through this historical land-use data. Manure N application data are obtained from Yang et al. (2016) at 5-arc × 5-arc min^2 resolution. DLEM also incorporates legume crops that fix atmospheric N (e.g., soybean and alfalfa). Biologically fixed N is simulated and added into the soil available N pools for crop uptake and N transformation. N from biomass turnover and residual after harvesting also enters into soil N pools and poses legacy effects for crops planted next year. The details of model input data and model structure can be found in the Supporting Information of Lu et al. (2020).

2.2. Partitioning Precipitation Into Heavy, Non-Heavy, and No-Precipitation Conditions

To partition precipitation events into "heavy," "non-heavy," and "no-precipitation" conditions, we define heavy precipitation when daily precipitation is over the monthly 90th percentiles. This definition allows spatial comparison across a large region and accounts for seasonality (Zhang et al., 2016). For easy comparison with extreme climate indices, the monthly 90th percentiles are estimated using all daily precipitation from days with precipitation greater than or equal to 1 mm in each month over the climatological baseline period 1961–1990. HP is identified at the grid cell level when the monthly 90th percentile threshold is surpassed. As a result, the days with

precipitation less than the 90th percentiles but larger than 1 mm are defined as non-heavy precipitation days. The days with precipitation less than or equal to 1 mm are defined as no-precipitation days.

2.3. Model Descriptions

Water and N yield: We use an improved version of the DLEM (version 2.0) that is developed to explicitly model carbon (C) and N cycling, water balances, vegetation structure and growth, and senescence dynamics of managed ecosystems (Liu et al., 2013; Lu et al., 2018; Tian et al., 2010; Yu et al., 2020). Particularly, the DLEM is capable of simulating water flow and N fluxes from land ecosystems (crops, grasslands, forests, etc.) to streams and rivers. The N considered in DLEM includes dissolved organic N (DON), dissolved inorganic N (DIN: NO_3-N and NH_4-N), and particulate organic N (PON). Since DIN constitutes over two-thirds of total N (TN) loading to the Northern Gulf of Mexico (Aulenbach et al., 2007; Scavia et al., 2017), we only quantify daily fluxes of DIN leaching and loading in this study. The representations of DIN leaching in DLEM are shown as following equations.

$$L_{NH4} = av_{NH4} \times Dis_{NH4} \times \frac{q_{srun} + q_{drain}}{W + q_{srun} + q_{drain}} / b_{NH4} \quad (6)$$

$$L_{NO3} = av_{NO3} \times Dis_{N03} \times \frac{q_{srun} + q_{drain}}{W + q_{srun} + q_{drain}} / b_{NO3} \quad (7)$$

where L_{NH4} and L_{NO3} are ammonia and nitrate leaching rates, av_{NH4} and av_{NO3} are soil available ammonia and nitrate, q_{srun} and q_{drain} are surface and subsurface runoff, W is soil moisture content, and b_{NH4} and b_{NO3} are plant-dependent parameters, representing the soil buffer effect of available N. Dis_{NH4} and Dis_{N03} are dissolving efficiency coefficients for NH_4 and NO_3, respectively, which are tuned in the model (by default it is 0.2 for NH_4-N and 1 for NO_3-N). The daily change in soil NH_4-N and NO_3-N pools is determined by the difference between N input (e.g., N deposition, N fertilizer use, manure N, biological N fixation) and N output (plant N uptake, nitrous gas emission, N leaching, and N loss due to other unknown pathways). The internal N transformation due to mineralization, immobilization, nitrification, and denitrification also contributes to partition N into reduced and oxidized inorganic N pools and organic N pools.

In DLEM, leached N is delivered from the land to water bodies along with water movement. The daily lateral fluxes of both water (e.g., surface runoff and sub-surface runoff) and N enter two logical water pools, namely surface water pool and drainage water pool, before flowing into streams and lakes. The simulating time step for water flux from the land to the water pools is 30 min. The N fluxes entering into the two pools are calculated based on allocation ratios that are determined by the surface runoff and sub-surface runoff. The details of the calculation can be found in Lu et al. (2020).

Land use and drought-induced crop mortality: Each grid cell in DLEM is a cohort of up to four natural plant functional types and one cropping system with its annual area percentage prescribed by land use input data. In this study, the distribution and physiological properties of corn, soybean, winter wheat, spring wheat, rice, and six other major crop types are specified across the MARB. The model is parameterized to approach the observations of annual gross primary production, and crop yields collected from multiple sites and county-level records across the United States (Lu et al., 2018; Yu et al., 2019). To characterize the impacts of severe drought, we add a module to represent crop mortality when drought intensity exceeds a threshold, which is based on air temperature and soil water content (Mananze et al., 2019).

Agricultural management practices: This version of DLEM also models the impacts of various agricultural management practices, including applications of synthetic N fertilizer and manure on crops, the effects of tile drainage on surface runoff, and the effects of technology innovations for crop yield improvement (Lu et al., 2018). The time-series gridded data of historical crop-specific N fertilizer use rate, timing, and types (e.g., NH_4-N and NO_3-N) are used to drive the DLEM model. Specifically, N fertilizer is applied at four timings in DLEM, namely before-planting (in spring before crop development), at-planting (in spring during crop planting), after-planting (early summer shortly after crop early development), and after-harvesting (late fall). The four N fertilizer timings are linked with the phenology for each fertilized crop type. The amount and type of applied N fertilizer at each timing a were derived from the reconstructed fertilizer management history data (Cao et al., 2018). Along with chemical N fertilizer data, manure N is applied based on the prescribed input data set. Our previous modeling

study has confirmed that the DLEM model captures the effects of N application amount and seasonality on the N yield and delivery from the MARB to the Gulf (Lu et al., 2020).

In DLEM, a percentage map of the tile-drained area is used to accelerate the water infiltration rate. The tile-drained land area percentage in a grid cell could range from 0% to 100% (Figure S1 in Supporting Information S1). The subsurface water flow is then accelerated by the adjusted infiltration rate, leading to faster runoff than the case without tile drainage. The impact of tile drainage is calibrated against the data from Malone et al. (2017). More details regarding tile drainage impacts can be found in Yu et al. (2018).

2.4. Model Calibration and Validation

We have calibrated the key parameters that regulate crop net primary productivity, soil organic C content, and water loss through evapotranspiration across multiple sites of the United States (Lu et al., 2018; Yu et al., 2018, 2019). In this study, we further calibrate parameters that control river discharge, soil N leaching, and riverine N loading. The simulated monthly streamflow and N loading to the Gulf of Mexico from 1980 to 2017 are validated by comparison with observed streamflow and N loading data obtained from the Mississippi River at St. Francisville, Louisiana (site ID 07373420) and Atchafalaya River at Melville, Louisiana (site ID 07381495) USGS monitoring sites and gauging stations (Figure S2 in Supporting Information S1). The USGS-derived riverine NO_2-N, NO_3-N, and NH_4-N data are based on the LOADEST software package (https://water.usgs.gov/software/loadest/). In addition to the model validation at the river outlet to the Gulf, we also validate the model's performance in simulating annual river discharge and N export for eight major subbasins of the MARB by comparing with the gauge-monitoring data obtained from the USGS (Table S1 in Supporting Information S1). DLEM estimates of river discharge and N load from these subbasins are close to the USGS LOADEST estimates over the years (Figure S3 in Supporting Information S1). To further test the model's performance in capturing peak streamflow and N loads, we compare the modeling results with the USGS LOADEST estimates across the eight subbasins when extremely high flows are recorded during 1980–2015 (https://toxics.usgs.gov/pubs/of-2007-1080/flux.html). The top 5% of high flow months (defined as exceeding the 95th percentile of observed flow rates) at the eight gauging stations are used to represent the high flow months. The modeling estimates of discharge and N loading from these subbasins are close to the USGS observations during extreme-flow months (Figure S4 in Supporting Information S1). To remove the uncertainty derived from the LOADEST approach, our previous work has validated the DLEM-modeled daily river discharge and N concentration against the daily raw observations from the USGS (Lu et al., 2020). Overall, this model is able to reproduce the daily, monthly and interannual variations in water discharge and N loading from the eight subbasins and the entire MARB.

2.5. Model Simulations

We project land-to-aquatic water yield and dissolved inorganic nitrogen (DIN) loads (including NH_4-N, NO_2-N, and NO_3-N) forward until 2099 using projected temperature, precipitation, and radiation from three CMIP5 ESMs under two RCP scenarios. All the simulations are forced by the transient climate from 1901 to 2099. Specifically, for the period 1901–2017, land use and land cover change, human agricultural management, and environmental drivers are based on the available databases introduced above. For the period 2018 to 2099, we keep all the environmental drivers but climate fixed to the 2017 level (e.g., N fertilizer input rates, N deposition, manure N rates, tile drainage, etc.). We also assume that the land use pattern will not change for the post-2017 period. To keep crop rotations for the future period, we repeatedly use the crop type maps of 2016 and 2017 for the years after 2018 to represent an "unchanged" crop rotation practice for the future period. The setups of static land-use and "maintaining-the-status" crop rotations allow us to distinguish and quantify the impacts of climate change and extreme climatic events on N loading, assuming current agricultural practices remain unchanged in the future. Furthermore, the simulation setups can highlight the potential drawbacks of current agricultural management practices on improving water quality given future climatic changes. We quantify N leaching to local waters at each grid as N yield (g N m^{-2} day^{-1}) and N delivered to rivers and coastal areas after in-stream transfer and decay as N loading (Tg N day^{-1}). Daily estimates are aggregated to the monthly or annual total for analysis and comparison purposes.

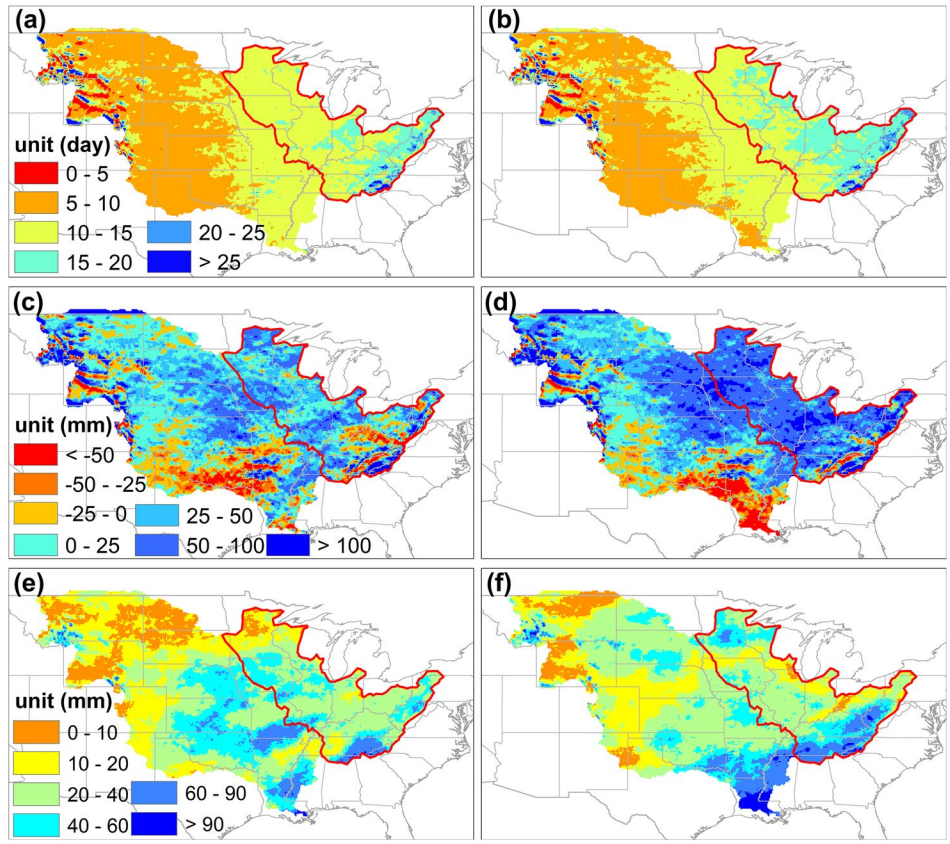

Figure 2. The number of days with heavy precipitation (HP) events each year averaged from 2070 to 2099 in the MARB under the RCP4.5 (a) and RCP8.5 (b) scenarios, the change of annual HP amount (mm) in the MARB between the periods of 2070–2099 and 1988–2017 under the RCP4.5 (c) and RCP8.5 (d) scenarios, and the standard deviation of the annual HP change (mm) among three Coupled Model Intercomparison Project 5 models under the RCP4.5 (e) and RCP8.5 (f) scenarios. The red outlines in sub-figures highlight the upper-Mississippi, mid-Mississippi River Basins, and the Ohio River Basin.

2.6. Summarizing Statistics

Changes in climate drivers (mainly precipitation-related), river discharge, N loading, water yield, and N yield are evaluated by the differences for these variables between the periods of 2070–2099 and 1988–2017. We report changes in the mean annual precipitation (mm), heavy precipitation frequency (days), and aridity (days), along with changes in mean annual river discharge and N loading (%) and yield of water (km^3) and N (Tg). Aridity is represented by the indices of consecutive dry days (CDDs), including annual total CDD, the longest CDD event, and the number of CDD events.

3. Results and Discussion

3.1. Changes in Precipitation in the MARB During the 21st Century

We first examine the patterns of future HP across the MARB for both RCP scenarios. The 30-year average annual HP from 2070 to 2099 across the MARB under the two climate scenarios shows a west-to-east gradient, ranging from less than 100 mm yr^{-1} in the west to ~600 mm yr^{-1} in the east (Figure S5 in Supporting Information S1). Although the annual TP is projected to remain relatively stable for both scenarios (Figure 1b), the annual total HP in the MARB on average would likely increase by 8% (±5%) and 15% (±8%) by the end of this century under the RCP4.5 and RCP8.5 scenarios, respectively (Table S2 in Supporting Information S1). HP amount is likely to increase substantially across the Upper Mississippi and Ohio River Basins where N fertilizer is intensively used to maximize crop yields of the US Corn Belt region (generally referring to Minnesota, Illinois, Indiana, Iowa, Nebraska, and Ohio; Figures 2a–2d). Only a small portion of the area lying within the southern MARB

is projected to experience a decrease (<−50 mm yr^{-1}) in HP amount under the examined scenarios (Figures 2c and 2d). However, the standard deviation (STD) of annual HP change shows a high variation (60–90 mm yr^{-1}) in the southern area of the MARB among the three CMIP5 models (Figures 2e and 2f). The spatial patterns of STD indicate that the predicted HP in this region has a larger uncertainty under both RCP scenarios, compared with the rest of MARB where the annual total HP STD is overall less than 60 mm yr^{-1} (Figures 2e and 2f). We further find that, between the two climate scenarios, the RCP8.5 scenario shows a larger spatial extent with HP increase >50 mm yr^{-1} than the RCP4.5 scenario (Figures 2c and 2d), despite an overall similar small increase in the number of HP events found in both scenarios (Figure S6 and Table S2 in Supporting Information S1).

3.2. Impacts of Future Precipitation Change on Water Yield and Nitrogen Loss in the MARB

Forced by climate prediction data from three CMIP5 models along with present-day agricultural practices and N fertilizer inputs, our simulation indicates that the river discharge is projected to only increase by 6 ± 3% (i.e., mean ± standard deviation among simulations driven by the three CMIP5 ESMs) under the RCP4.5 and nearly zero-change with a large among-model variation (0.3 ± 5%) under the RCP8.5 scenarios (Figure 3a). However, the MARB annual N loading would increase by ∼30% during the last three decades of the 21st century under the RCP4.5 (30 ± 3%) and the RCP8.5 (31 ± 14%) scenarios, compared to the most recent three decades (Figure 3b). All other input drivers being equal, model simulations indicate that the estimated discharge and N loading show a larger uncertainty under the RCP8.5 scenario than the RCP4.5 scenario (Figures 3a and 3b), corresponding to the divergence among future climate projections. Using projected climate from six CMIP5 ESMs under the RCP8.5 scenario, Kujawa et al. (2020) demonstrated that variation among climate models was the dominant source of uncertainty in predicting future total discharge and total N loading in a watershed located in northwest Ohio. This study supports our findings regarding uncertainty sources in projected discharge and N loading in the MARB.

To gain insights into the impacts of future precipitation changes on N export, we quantify the contributions of HP events, non-HP events, and no-precipitation days to water yield (i.e., the sum of surface runoff and drainage runoff) and N yield (i.e., N leaching from soils) across the MARB. Under the RCP4.5 scenario, HP-induced water yield change (49.1 ± 16.8 km^3 yr^{-1}) would dominate the total water yield increase (44.8 ± 20.3 km^3 yr^{-1}; Figure 3c and Table S3 in Supporting Information S1). For the RCP8.5 scenario, while the water yield increase on the HP days is more robust (64.1 ± 16.4 km^3 yr^{-1}), it is offset by the decreases in water yield during non-HP days (−35.5 ± 19.9 km^3 yr^{-1}) and no-precipitation days (−25.3 ± 18 km^3 yr^{-1}). The offset of daily water yield leads to a small net increase in the annual total water yield (3.3 ± 32.6 km^3 yr^{-1}) under the RCP8.5 scenario, despite a large among-model variation (Figure 3c and Table S3 in Supporting Information S1).

Along with the total water yield increase, the projected change in total N yield would increase up to 0.55 (±0.11) Tg yr^{-1} for the RCP4.5 scenario (Figure 3d). Surprisingly, despite the small increase in total water yield, the projected total N yield would increase by 0.68 (±0.33) Tg yr^{-1} under the RCP8.5 scenario (Figure 3d). Specifically, we find that the N yield increases in HP days would on average account for 45% (0.25 ± 0.05 Tg yr^{-1}) and 56% (0.38 ± 0.18 Tg yr^{-1}) of the total N yield increase under the RCP4.5 and the RCP8.5 scenarios, respectively (Figure 3d and Table S4 in Supporting Information S1). With the changes in the HP-induced water yield (Figure 3c), our modeling results highlight the significant roles of future HP in contributing N yield across the MARB (Figure 3d). The results for the RCP8.5 scenario indicate that the riverine N concentration would increase, which likely drives the further deterioration of water quality in the region (Davidson et al., 2011).

Furthermore, the projected changes of N yield also highlight the critical role of days without precipitation in flushing out N, particularly under the RCP8.5 scenario (Figure 3d). Specifically, the N yield from no-precipitation days would account for 39% (0.21 ± 0.07 Tg yr^{-1}) and 37% (0.25 ± 0.15 Tg yr^{-1}) of the total N yield increase under the RCP4.5 and RCP8.5 scenarios, respectively (Figure 3d and Table S4 in Supporting Information S1). These findings indicate the significant legacy effects after rainfall events on N yield under future climate conditions.

Compared with HP and no-precipitation events, the small increases in non-HP frequency and intensity (Table S4 in Supporting Information S1) would accordingly play a smaller role in determining N yield, only accounting for 16% (0.09 ± 0.02 Tg yr^{-1}) and 8% ± (0.05 ± 0.02 Tg yr^{-1}) of total N yield increases under the RCP4.5 and RCP8.5 scenarios, respectively (Figure 3d and Table S4 in Supporting Information S1). This is likely due to longer drought periods and the decreases in the number of non-HP events by the end of the century (Figure

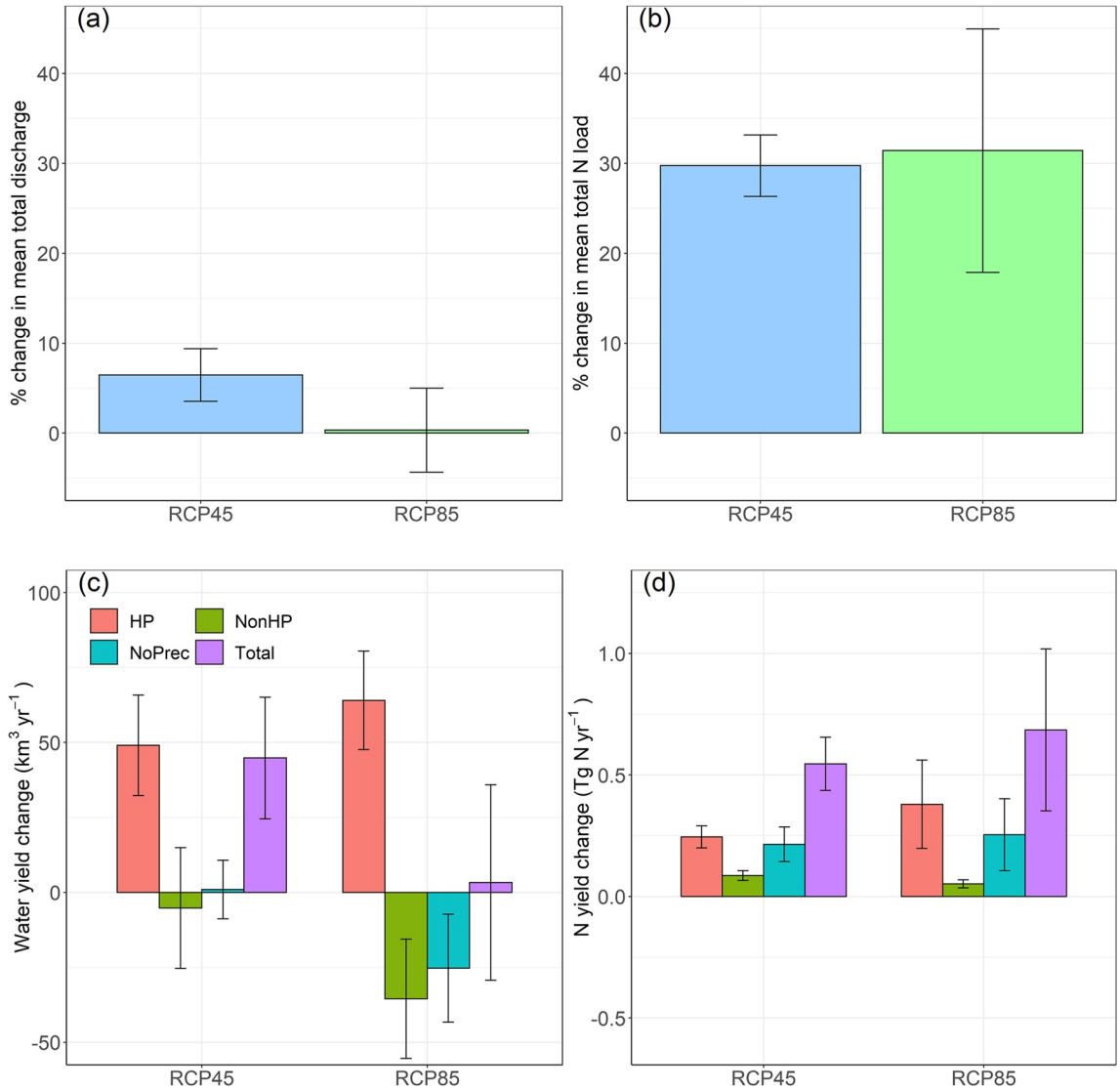

Figure 3. Predicted changes in annual river discharge, N loading, water yield (i.e., the sum of surface and subsurface runoff), and N yield (i.e., N leaching from soils, calculated as a sum of all simulation grids) from the MARB at the end of the century under the RCP4.5 and RCP8.5 scenarios. (a, b) The change of annual total river discharge (a) and annual total N loading (b) at the river outlets to the Gulf of Mexico is calculated as the difference between the periods of 2070–2099 and 1988–2017 under the RCP4.5 and RCP8.5 scenarios. (c, d) The change of water yield (c) and N yield (d) occurred in HP days, non-HP days, and no-precipitation days is calculated as the difference between the periods of 2070–2099 and 1988–2017 under the two climate scenarios. The error bars are the standard deviation among DLEM model simulations driven by climate scenario data from the three Coupled Model Intercomparison Project 5 models.

S7 in Supporting Information S1). It is also noteworthy that our predictions have large among-model variations, especially for the RCP8.5 scenario (Figure 3).

The seasonality of N fluxes in the MARB promotes the development of extensive seasonal hypoxia in the Gulf of Mexico (Donner & Kucharik, 2008) and has important implications for upstream agricultural management selection and planning (e.g., fertilizer application; Wine et al., 2020). We therefore quantify seasonal changes in N loading from the Basin. About 41% and 51% (i.e., 0.12 and 0.15 Tg N season^{-1}) of the annual N loading increase would come from spring under the RCP4.5 and RCP8.5 scenarios, respectively (Figure 4). In the presence of recurrent anthropogenic N fertilizer input across the MARB, increases in spring precipitation (Figure S8a in Supporting Information S1) would cause a higher N yield from land (Figure S8b in Supporting Information S1). It is noteworthy that the increase in HP-induced N yield would account for 47% (RCP4.5) and 50% (RCP8.5) of the spring total N yield increase (Figure S8b in Supporting Information S1), which is likely the major driver for the spring N loading increase. The increase in N loading over the summer months would be ~26% (i.e., ~0.08 Tg

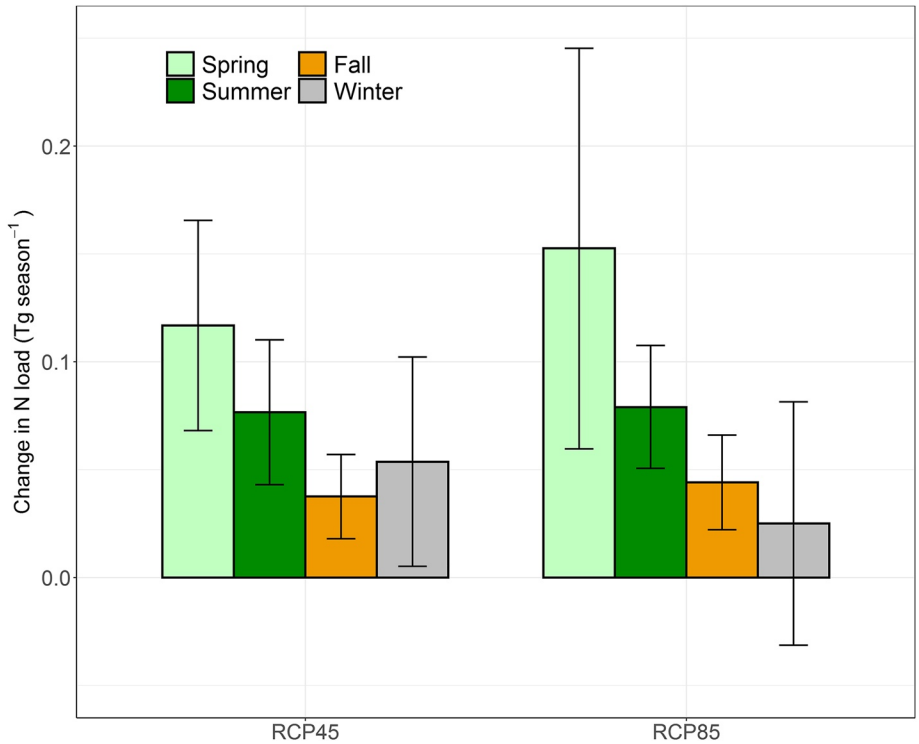

Figure 4. Predicted changes in seasonal total N loading from the MARB at the end of the century under the RCP4.5 and RCP8.5 scenarios. The change of N loading indicates how far the predicted N loadings during 2070–2099 under the RCP4.5 and the RCP8.5 scenarios are away from the historical model-estimated N loading during 1988–2017. Spring: March, April, and May (MAM); Summer: June, July, and August (JJA); Fall: September, October, and November (SON); Winter: December, January, and February (DJF). The error bars are the standard deviation of DLEM-estimated N loading changes driven by climate scenario data from three Coupled Model Intercomparison Project 5 models.

season^{-1}) of the annual N loading increase under both RCP scenarios, which is mainly driven by non-heavy precipitation (Figure S8 in Supporting Information S1). Although lower future N loading increases tend to occur in fall and winter (Figure 4), they would be driven by increases in HP during low discharge periods (Figure S8 in Supporting Information S1). Model simulations present that the estimated seasonal changes in N loading have a larger uncertainty under both RCP scenarios, especially in spring, which is due to the divergence among future climate projections.

3.3. Spatial Patterns of Water Yield and Nitrogen Yield Across the MARB

Widespread increases in total water yield by the end of the century are predicted across the MARB under the two future scenarios (Figures 5a and 5b). The predicted increases in total N yield in the upper-Mississippi and mid-Mississippi River Basins stand out under both RCP scenarios (Figures 5e and 5f) despite the predicted increases of annual aridity (Figure S7 in Supporting Information S1). These regions are the home to more than half of the US agricultural production (Yu & Lu, 2018), where more N fertilizer is applied than anywhere else in the United States (Cao et al., 2018; Lu et al., 2019; Zhang, Cao, et al., 2021). Specifically, the water yield increases on the HP days under the RCP8.5 scenario would be more spatially extended than those under the RCP4.5 scenario (Figures 5c and 5d), leading to an overall higher N yield (Figures 5g and 5h), especially in the upper-Mississippi River Basin. The Mississippi Alluvial Plain (referring to the region with the highest rice production in the southern four states, including Arkansas, Louisiana, Mississippi, and Texas, in the United States) in the southern MARB also displays significant increases in N yield when HP events would occur in the future (Figures 5c and 5d).

We also find that water yield on the non-HP days would decline over a large portion of the MARB, while the declines in N yield would not be as widespread as water yield (Figures S9a, S9b, S10a, and S10b in Supporting

10.1029/2021EF002141

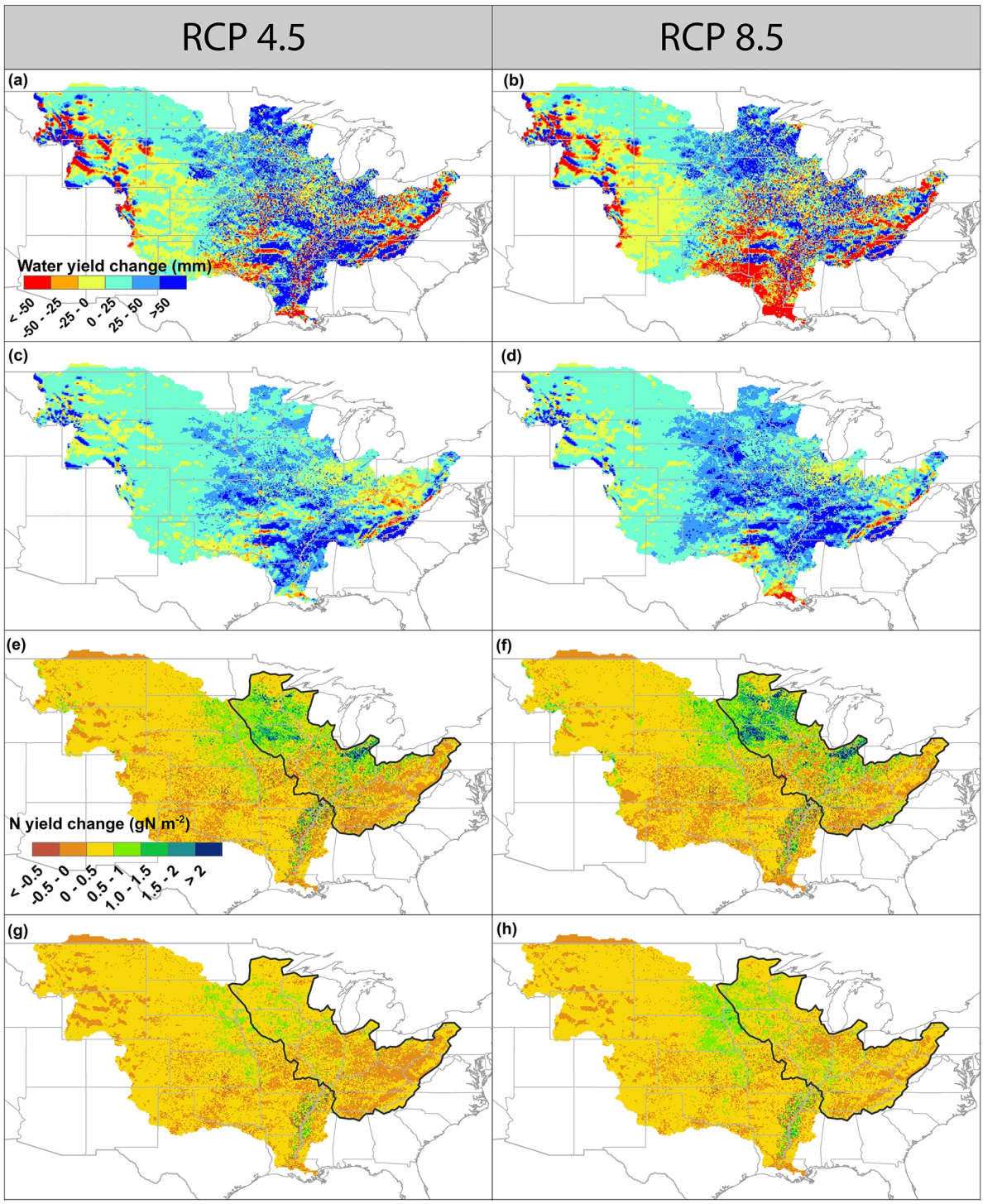

Figure 5. Predicted changes in total water yield and total N yield at the end of the century. The predicted changes in annual total water yield (a) and (b) and water yield in HP days (c) and (d) between the periods of 2070–2099 and 1988–2017 under the RCP4.5 (a, c) and RCP8.5 (b, d) scenarios. The predicted change in annual total N yield (e) and (f) and N yield in HP days (g) and (h) between the periods of 2070–2099 and 1988–2017 under the RCP4.5 (e, g) and RCP8.5 (f, h) scenarios. The black outlines in sub-figures (e–h) highlight the upper-Mississippi, mid-Mississippi River Basins, and the Ohio River Basin.

Information S1). It is noteworthy that, on no-precipitation days, the areas with declined water yield would be mainly located in the southern and western MARB and would be larger than the areas with increases in water yield (Figures S9c and S9d in Supporting Information S1). These water yield changes over space lead to a basin-wide negligible change and a slight decrease in water yield under the RCP4.5 and the RCP8.5 scenarios,

respectively (Figure 5c). However, increased water yield (Figures S9c and S9d in Supporting Information S1), continued intensive fertilizer use, and a greater preponderance of tile drainage in the agriculture-dominated watersheds in the Midwest would together drive robust N yield during the no-precipitation days for the two RCP scenarios (Figures S10c and S10d in Supporting Information S1). These hotspots indicate the potential legacy effects after rainfall events on N yield, depending on the regions and N input amount applied to the cropland surface (Van Meter et al., 2016, 2017, 2018).

3.4. Spatial Variations of Water Yield and Nitrogen Yield

Our results indicate that future climate conditions associated with the high-emission scenario would bring a bigger challenge for the stakeholders to reduce N leaching in the MARB. This conclusion is supported by a recent study (Sinha et al., 2017), which focused on exploring the annual and seasonal patterns of precipitation in determining N load. Divergences in precipitation projections among CMIP5 models translate into large variations in the magnitude of predicted water and N yield changes across the MARB (Figures S11–S13 in Supporting Information S1), illustrating the importance of reducing uncertainties in the future climate projections (Sinha et al., 2017). For water yield induced by HP events, the central and southeastern MARB display the largest among-model variations (e.g., up to 110 mm yr^{-1} and 120 mm yr^{-1} under the RCP4.5 and RCP8.5 scenarios, respectively; Figures S11a and S11b in Supporting Information S1). Large variations in N yield are also found in both the Corn Belt and the Mississippi Alluvial Plain under future scenarios (Figures S11c and S11d in Supporting Information S1). Specifically, the highest N yield variation would likely occur in the Mississippi Alluvial Plain, which would reach up to 0.8 and 2.4 g N m^{-2} yr^{-1} under the RCP4.5 and the RCP8.5 scenarios, respectively. Compared with the RCP4.5 scenario, a larger spatial extent of N yield variation is found under the RCP8.5 scenario. These spatial patterns of N yield variations highlight the challenges to implementing region-specific N mitigation practices in watersheds with high N inputs and more frequent and extreme precipitation (Figure S12 in Supporting Information S1). Also, future studies should pay more attention to the uncertainties in predicting HP-induced water yield and N yield using climate models from the CMIP5 ensemble.

Compared with the HP days, the among-model variations in water yield (e.g., <40 mm yr^{-1}) and N yield (e.g., <0.6 g N m^{-2} yr^{-1}) during the non-HP days present a lower magnitude and a smaller extent across the Basin (Figures S12 and S13 in Supporting Information S1). This implies that the non-HP predictions are relatively convergent among the three CMIP5 models, and so are their impacts on future water and N yields. Although the spatial extent of water and N yield variations under no-precipitation days are smaller than those under the HP days, higher variation magnitudes (e.g., >40 mm yr^{-1} for water yield; >0.6 g N m^{-2} yr^{-1} for N yield) are detected in the Midwestern states like Iowa and Indiana (Figure S13 in Supporting Information S1). Between the two RCP scenarios, the water yield and N yield during the non-HP days and no-precipitation days would be more variable under the RCP8.5 scenario. These spatial variations suggest that heavy precipitation would play a significant role in determining future water and N yields. However, the climate models contain large uncertainties in predicting the occurrence and severity of heavy rainfall events.

4. Uncertainties and Limitations

Our study involves uncertainties in the following aspects. First, uncertainties existing in the 21st-century CMIP5 precipitation projections dominate the uncertainties of predicted water and N yields across the MARB. These sources of CMIP5 projection uncertainty are generally classified into three types: internal variability, inter-model variability, and greenhouse gas emissions (Chen et al., 2014). Kharin et al. (2013) shows that confidence in the projected changes in extreme precipitation is low in the tropics due to the large inter-model disagreements, indicating that some physical processes associated with extreme precipitation may not be well represented in the current generation of models. Our uncertainty analyses of changes in future HP, water yield, and N yield also demonstrate a relatively high inter-model disagreement in the southern parts of the Basin (Figures S5c, S5cd, and S11–S13 in Supporting Information S1). Using CMIP5 models, Chen et al. (2014) finds that inter- and intra-model variability are the dominant sources of uncertainty in global precipitation-related extremes. However, the increases in intensified extreme precipitation occurring in North America detected in the CMIP5 models demonstrate a higher inter-model agreement than other regions around the globe (Chen et al., 2014). Therefore, the uncertainties of modeled water and N yields across the MARB presented in our study are highly driven

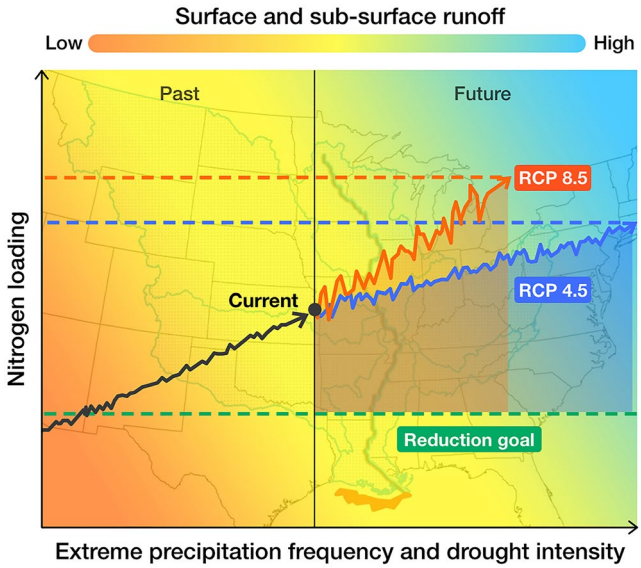

Figure 6. Conceptual diagram of possible trajectories of nitrogen (N) loading changes induced by heavy rainfall intensity and frequency under future climate and management scenarios. The trajectory of N loading illustrated in this figure is not a reflection of the real-world annual total N loading trend in the MARB but is used to represent the potential "cause-effect" between N loading and increases in heavy rainfall frequency and intensity in the Basin. As indicated by this study, the RCP8.5 scenario is likely to yield a smaller increase of runoff but a larger N loading than the RCP4.5 scenario under the same level of anthropogenic N input.

by uncertainties in future climate projections, particularly for the HP events. Systematic analyses of N load uncertainty sources deserve further research efforts.

Second, our analyses only consider the same-day HP-induced water and N yields. Soil water content can be largely increased by extreme rainfall events and persists over the following days, leading to a consistently high baseflow and consequently high N leaching for several days. In our analysis, however, we classify the N yield following the HP events into the N yield occurring on non-HP or no-precipitation days. This assumption potentially underestimates the "HP-induced" N yield and load but overestimates those occurring on other days. Therefore, our modeled N loads can be treated as a lower estimation bound of the real-world N loads induced by HP events. Based on our conservative modeling estimates, we can foresee that the extreme N loads and eutrophication peaks in the Gulf would likely be larger after future extreme precipitation events. Effects on water quality of extreme precipitation, and of its legacy, merit further analysis.

Third, N fertilizer input data used by our model relies on the state-level crop-specific N fertilizer use survey, assuming N fertilizer applied to the same crops is at a uniform rate within a state. Due to limited information, we multiply the N fertilizer use rate by the state-level crop-specific fertilized area percentage (e.g., 98% of corn is fertilized and 2% is non-fertilized in Iowa, Lu et al. (2019)). This step "dilutes" the fertilizer input while guaranteeing the total N fertilizer amount is consistent with the state-level survey data. Nevertheless, the consequence of this modification leads to a case that the areas without N fertilization would also receive the same state-level N input rate as other fertilized areas in that state. Although the unfertilized area is very low for most crops, the spatial extent of N yield and loading estimated in our study would likely be overestimated across the Basin, while the magnitude is underestimated in fertilized soils. Crop-specific N fertilizer use rates at a finer spatial scale (e.g., field-level) can be essential for improving the prediction accuracy of excess N load in a changing climate.

5. Recommendations for Future N Management in the MARB

Concentrated precipitation bursts with durations of a few hours are projected to be more common (Westra et al., 2013). Increases in extreme precipitation are likely to be accompanied by increases in extreme nutrient loading (Carpenter et al., 2018). As Figure 6 demonstrates, our modeling results suggest that precipitation changes in agricultural regions would likely intensify N pollution in the Gulf of Mexico by the end of the century. As temperature increases (Figure 1a) and precipitation becomes more variable and extreme (Figure 1b and Figure S5 in Supporting Information S1), droughts would become more common under the RCP8.5 scenario (Figure S7 in Supporting Information S1), which can intensify N loading and its variation (Figure 6). Drought decreases N loading due to short-term low water flows. However, rapid transitions from dry to wet conditions lead to increased N fluxes (Loecke et al., 2017). Inorganic N that is easily mobilized may accumulate in the soil during drought periods. Subsequent heavy or non-heavy rainfall events could exacerbate N leaching by flushing out the unused residual soil N (Lee et al., 2016; Morecroft et al., 2000; Shepherd et al., 2018; Zhang, Lu, et al., 2021).

It is also important to emphasize that the current agricultural production systems would likely adapt to the changes in total precipitation, heavy precipitation, and seasonal patterns. Much of the Corn Belt region receives more-than-adequate precipitation during the growing season, and the landscape has been hydrologically altered to hasten the transfer of water to the stream network (Dai et al., 2016; Kelly et al., 2017; Munoz et al., 2018) to maximize crop production. These alterations, which include stream straightening, ditch construction, drainage of wetlands, and lowering the water table using subsurface networks of porous pipes, have magnified agricultural N loss and downstream eutrophication (Skaggs et al., 1994). DIN loading in May is the best predictor of the areal extent of summer hypoxia in the Gulf of Mexico (Turner et al., 2006). As heavy precipitation would increase in

spring (Figure S8a in Supporting Information S1), Corn Belt farmers are likely to intensify their drainage practices (Singh et al., 2009) and increase N inputs (Houser et al., 2019) while attempting to maintain production levels, multiplying the effects of climate change alone on N loads and hypoxia in summer. Particularly in the Midwest, the majority of N fertilizer is applied before crops are planted. For example, corn N fertilizer application before crop planting (in spring only) accounts for 43% of annual N fertilizer usage in Iowa and 59% in Minnesota, and the amounts of N fertilizer applied at crop planting (9% in Iowa and 5% in Minnesota), after crop planting (25% and 4%), and after crop harvest (in the fall of the previous year, 23% and 32%) are all less than that applied in spring before crop planting (Cao et al., 2018). With the current N input strategy, increases in heavy precipitation are likely to cause increases in N loading, especially in spring when before-planting and at-planting N fertilizer are applied (Figure 4 and Figure S8 in Supporting Information S1). We find that near a half of the annual total N yield increase across the basin would be from spring (37% under the RCP4.5% and 40% under the RCP8.5 scenarios). Hence land managers should adopt more aggressive management intervention and advanced technologies, such as monitoring crop N demands for precision fertilizer use, using slow-releasing fertilizer type, to reduce the adverse impacts of heavy precipitation events while maintaining crop production. Additionally, side-dressing and postponing fall as well as spring before-planting fertilizer application until crop germinates could be effective to lessen the risk of N loss under heavy rainfall events (Lu et al., 2020). Nevertheless, an existing study argued that the CMIP5 climate models tend to overestimate the number of spring extreme precipitation events and underestimate summer events in the contiguous United States compared to observations (e.g., summer events were underestimated by 16% and spring events overestimated by 14% in the Midwestern United States; Janssen et al., 2016). This might slightly contribute to the large spring increases in the N yield and loading estimated in our study. The effects of climate and land management on nutrient export from agricultural systems remain as the current research challenge that involves multiple climatic variables, landscape heterogeneity, and agricultural practices (Deshmukh & Singh, 2016; Frans et al., 2013; Gupta et al., 2015; Martin et al., 2017; Shang, 2019). More research is needed to clarify the roles of heavy precipitation changes versus agricultural management (e.g., rotation, tile drainage, N fertilizer application timing, etc.) for nutrient loading. To reach the reduction goals of N load and hypoxia in the Gulf of Mexico, we need to take the trajectories of future extreme climate into account to assess and improve the mitigation efforts.

Our conclusions drawn here have global implications for watershed nutrient management and eutrophication reduction in the coasts, given the future changing climate and enhanced hydroclimatic extreme events. Our recent analyses reveal that more extreme precipitation events have been projected to occur in the upper-Mississippi River Basin where N fertilizers are used more intensively (Lu et al., 2020). Understanding the extreme climate trends could inform farm-management practices and lessen the likelihood of N loading in waterways. For example, land managers may use cover crops to enhance long-term ecosystem N retention capability, reduce N input amount using rotation system, and modify fertilizer application timing to meet crop nutrient demands while minimizing the contribution of extreme precipitation events. We have demonstrated that historical N loading from the MARB to the Gulf of Mexico could be reduced by up to 16% if N fertilizers are applied multiple times after crops develop, without affecting crop productivity (Lu et al., 2020). To achieve the feasibility of water pollution mitigation, we call for more studies are needed to interpret the relative effects of extreme climate and land management practices, such as cover crops, riparian buffers, side-dressed N fertilizer, precision N management, and so on, on N outputs from agricultural watersheds.

Conflict of Interest

The authors declare no conflicts of interest relevant to this study.

Data Availability Statement

The data supporting the major findings of this study, including annual average climate conditions as well as the statistics of model-estimated river discharge, N load, water, and N yield across the Basin can be found in https://doi.org/10.6084/m9.figshare.19394132.v1. The raw model outputs from this study are accessible upon request (contact: clu@iastate.edu)

Acknowledgments
This work is supported partially by Iowa Nutrient Research Center, the NSF grant (1903722), the NSF CAREER (1945036), and the Iowa State University postdoc seed grant. The authors thank the two anonymous reviewers for improving the manuscript.

References

Abatzoglou, J. T. (2013). Development of gridded surface meteorological data for ecological applications and modelling. *International Journal of Climatology*, *33*(1), 121–131.

Abatzoglou, J. T., & Brown, T. J. (2012). A comparison of statistical downscaling methods suited for wildfire applications. *International Journal of Climatology*, *32*(5), 772–780.

Aulenbach, B. T., Buxton, H. T., Battaglin, W. A., & Coupe, R. H. (2007). *Streamflow and nutrient fluxes of the Mississippi-Atchafalaya River Basin and subbasins for the period of record through 2005*. US Geological Survey.

Ballard, T. C., Sinha, E., & Michalak, A. M. (2019). Long-term changes in precipitation and temperature have already impacted nitrogen loading. *Environmental Science & Technology*, *53*(9), 5080–5090.

Cao, P., Lu, C., & Yu, Z. (2018). Historical nitrogen fertilizer use in agricultural ecosystems of the contiguous United States during 1850–2015: Application rate, timing, and fertilizer types. *Earth System Science Data*, *10*(2), 969–984.

Carpenter, S. R., Booth, E. G., & Kucharik, C. J. (2018). Extreme precipitation and phosphorus loads from two agricultural watersheds. *Limnology & Oceanography*, *63*(3), 1221–1233.

Chen, H., Sun, J., & Chen, X. (2014). Projection and uncertainty analysis of global precipitation-related extremes using CMIP5 models. *International Journal of Climatology*, *34*(8), 2730–2748.

Clarke, L., Edmonds, J., Jacoby, H., Pitcher, H., Reilly, J., & Richels, R. (2007). *Scenarios of greenhouse gas emissions and atmospheric concentrations*.

Collins, W. J., Bellouin, N., Doutriaux-Boucher, M., Gedney, N., Halloran, P., Hinton, T., et al. (2011). Development and evaluation of an Earth-System model – HadGEM2. *Geoscientific Model Development Discussions*, *4*(2), 997–1062.

Dai, S., Shulski, M. D., Hubbard, K. G., & Takle, E. S. (2016). A spatiotemporal analysis of Midwest US temperature and precipitation trends during the growing season from 1980 to 2013. *International Journal of Climatology*, *36*(1), 517–525.

Davidson, E. A., David, M. B., Galloway, J. N., Goodale, C. L., Haeuber, R., Harrison, J. A., et al. (2011). Excess nitrogen in the US environment: Trends, risks, and solutions. *Issues in Ecology*, (15).

Dentener, F. J. (2006). *Global Maps of Atmospheric Nitrogen Deposition, 1860, 1993, and 2050*. Oak Ridge, TN: ORNL DAAC. https://doi.org/10.1016/j.ridd.2011.06.019

Deshmukh, A., & Singh, R. (2016). Physio-climatic controls on vulnerability of watersheds to climate and land use change across the US. *Water Resources Research*, *52*(11), 8775–8793.

Donner, S. D., & Kucharik, C. J. (2003). Evaluating the impacts of land management and climate variability on crop production and nitrate export across the Upper Mississippi Basin. *Global Biogeochemical Cycles*, *17*(3).

Donner, S. D., & Kucharik, C. J. (2008). Corn-based ethanol production compromises goal of reducing nitrogen export by the Mississippi River. *Proceedings of the National Academy of Sciences of the United States of America*, *105*(11), 4513–4518.

Dunne, J. P., John, J. G., Shevliakova, E., Stouffer, R. J., Krasting, J. P., Malyshev, S. L., et al. (2013). GFDL's ESM2 global coupled climate–carbon Earth system models. Part II: Carbon system formulation and baseline simulation characteristics. *Journal of Climate*, *26*(7), 2247–2267.

Evans, A. E. V., Hanjra, M. A., Jiang, Y., Qadir, M., & Drechsel, P. (2012). Water quality: Assessment of the current situation in Asia. *International Journal of Water Resources Development*, *28*(2), 195–216.

Frans, C., Istanbulluoglu, E., Mishra, V., Munoz-Arriola, F., & Lettenmaier, D. P. (2013). Are climatic or land cover changes the dominant cause of runoff trends in the Upper Mississippi River Basin? *Geophysical Research Letters*, *40*(6), 1104–1110.

Grizzetti, B., Bouraoui, F., Billen, G., vanGrinsven, H., Cardoso, A. C., Thieu, V., et al. (2011). *Nitrogen as a threat to European water quality*.

Gupta, S. C., Kessler, A. C., Brown, M. K., & Zvomuya, F. (2015). Climate and agricultural land use change impacts on streamflow in the upper midwestern United States. *Water Resources Research*, *51*(7), 5301–5317.

Houser, M., Gunderson, R., & Stuart, D. (2019). Farmers' perceptions of climate change in context: Toward a political economy of relevance. *Sociologia Ruralis*, *59*(4), 789–809.

Howarth, R. W., Anderson, D., Cloern, J., Elfring, C., Hopkinson, C., Lapointe, B., et al. (2000). Nutrient pollution of coastal rivers, bays, and seas. *Issues in Ecology*, *7*, 1–15. http://pubs.er.usgs.gov/publication/70185674

Howarth, R. W., & Marino, R. (2006). Nitrogen as the limiting nutrient for eutrophication in coastal marine ecosystems: Evolving views over three decades. *Limnology & Oceanography*, *51*(1part2), 364–376.

Howarth, R. W., Swaney, D. P., Boyer, E. W., Marino, R., Jaworski, N., & Goodale, C. (2006). The influence of climate on average nitrogen export from large watersheds in the Northeastern United States. In *Nitrogen cycling in the Americas: Natural and anthropogenic influences and controls* (pp. 163–186). Springer.

Janssen, E., Sriver, R. L., Wuebbles, D. J., & Kunkel, K. E. (2016). Seasonal and regional variations in extreme precipitation event frequency using CMIP5. *Geophysical Research Letters*, *43*(10), 5385–5393.

Kelly, S. A., Takbiri, Z., Belmont, P., & Foufoula-Georgiou, E. (2017). Human amplified changes in precipitation-runoff patterns in large river basins of the Midwestern United States. *Hydrology and Earth System Sciences*, *21*(10), 5065–5088. https://doi.org/10.5194/hess-21-5065-2017

Kharin, V. V., Zwiers, F. W., Zhang, X., & Wehner, M. (2013). Changes in temperature and precipitation extremes in the CMIP5 ensemble. *Climatic Change*, *119*(2), 345–357.

Kujawa, H., Kalcic, M., Martin, J., Aloysius, N., Apostel, A., Kast, J., et al. (2020). The hydrologic model as a source of nutrient loading uncertainty in a future climate. *The Science of the Total Environment*, *724*, 138004.

Lee, M., Shevliakova, E., Malyshev, S., Milly, P. C. D., & Jaffé, P. R. (2016). Climate variability and extremes, interacting with nitrogen storage, amplify eutrophication risk. *Geophysical Research Letters*, *43*(14), 7520–7528. https://doi.org/10.1002/2016GL069254

Liu, M., Tian, H., Yang, Q., Yang, J., Song, X., Lohrenz, S. E., & Cai, W. J. (2013). Long-term trends in evapotranspiration and runoff over the drainage basins of the Gulf of Mexico during 1901-2008. *Water Resources Research*, *49*(4), 1988–2012. https://doi.org/10.1002/wrcr.20180

Loecke, T. D., Burgin, A. J., Riveros-Iregui, D. A., Ward, A. S., Thomas, S. A., Davis, C. A., & Clair, M. A. S. (2017). Weather whiplash in agricultural regions drives deterioration of water quality. *Biogeochemistry*, *133*(1), 7–15.

Lu, C., & Tian, H. (2017). Global nitrogen and phosphorus fertilizer use for agriculture production in the past half century: Shifted hot spots and nutrient imbalance. *Earth System Science Data*, *9*(1), 181–192.

Lu, C., Yu, Z., Tian, H., Hennessy, D. A., Feng, H., Al-Kaisi, M., et al. (2018). Increasing carbon footprint of grain crop production in the US Western Corn Belt. *Environmental Research Letters*, *13*(12), 124007.

Lu, C., Zhang, J., Cao, P., & Hatfield, J. (2019). Are we getting better in using nitrogen?: Variations in nitrogen use efficiency of two cereal crops across the United States. *Earth's Future*, *7*(8), 939–952. https://doi.org/10.1029/2019EF001155

Lu, C., Zhang, J., Tian, H., Crumpton, W. G., Helmers, M. J., Cai, W.-J., et al. (2020). Increased extreme precipitation challenges nitrogen load management to the Gulf of Mexico. *Communications Earth & Environment*, *1*(1), 21. https://doi.org/10.1038/s43247-020-00020-7

Malone, R. W., Kersebaum, K. C., Kaspar, T. C., Ma, L., Jaynes, D. B., & Gillette, K. (2017). Winter rye as a cover crop reduces nitrate loss to subsurface drainage as simulated by HERMES. *Agricultural Water Management*, *184*, 156–169.
Mananze, S., Pôças, I., & Cunha, M. (2019). Agricultural drought monitoring based on soil moisture derived from the optical trapezoid model in Mozambique. *Journal of Applied Remote Sensing*, *13*(2), 24519.
Martin, K. L., Hwang, T., Vose, J. M., Coulston, J. W., Wear, D. N., Miles, B., & Band, L. E. (2017). Watershed impacts of climate and land use changes depend on magnitude and land use context. *Ecohydrology*, *10*(7), e1870.
Mesinger, F., DiMego, G., Kalnay, E., Mitchell, K., Shafran, P. C., Ebisuzaki, W., et al. (2006). North American regional reanalysis. *Bulletin of the American Meteorological Society*, *87*(3), 343–360.
Mitchell, T. D., & Jones, P. D. (2005). An improved method of constructing a database of monthly climate observations and associated high-resolution grids. *International Journal of Climatology*, *25*(6), 693–712. https://doi.org/10.1002/joc.1181
Morecroft, M. D., Burt, T. P., Taylor, M. E., & Rowland, A. P. (2000). Effects of the 1995–1997 drought on nitrate leaching in lowland England. *Soil Use & Management*, *16*(2), 117–123.
Munoz, S. E., Giosan, L., Therrell, M. D., Remo, J. W. F., Shen, Z., Sullivan, R. M., et al. (2018). Climatic control of Mississippi River flood hazard amplified by river engineering. *Nature*, *556*(7699), 95–98.
National Academies of Sciences, Engineering, and Medicine. (2016). *Attribution of extreme weather events in the context of climate change*. National Academies Press.
Rabalais, N. N., Turner, R. E., Sen Gupta, B. K., Boesch, D. F., Chapman, P., & Murrell, M. C. (2007). Hypoxia in the northern Gulf of Mexico: Does the science support the plan to reduce, mitigate, and control hypoxia? *Estuaries and Coasts*, *30*, 753–772. https://doi.org/10.1007/BF02841332
Riahi, K., Grübler, A., & Nakicenovic, N. (2007). Scenarios of long-term socio-economic and environmental development under climate stabilization. *Technological Forecasting and Social Change*, *74*(7), 887–935.
Riahi, K., Rao, S., Krey, V., Cho, C., Chirkov, V., Fischer, G., et al. (2011). RCP 8.5—A scenario of comparatively high greenhouse gas emissions. *Climatic Change*, *109*(1), 33–57.
Scavia, D., Bertani, I., Obenour, D. R., Turner, R. E., Forrest, D. R., & Katin, A. (2017). Ensemble modeling informs hypoxia management in the northern Gulf of Mexico. *Proceedings of the National Academy of Sciences of the United States of America*, *114*(33), 8823–8828. https://doi.org/10.1073/pnas.1705293114
Shang, L. (2019). *Climate change and land use/cover change impacts on watershed hydrology, nutrient dynamics—A case study in Missisquoi River watershed*.
Shepherd, M., Lucci, G., Vogeler, I., & Balvert, S. (2018). The effect of drought and nitrogen fertiliser addition on nitrate leaching risk from a pasture soil: An assessment from a field experiment and modelling. *Journal of the Science of Food and Agriculture*, *98*(10), 3795–3805.
Singh, R., Helmers, M. J., Kaleita, A. L., & Takle, E. S. (2009). Potential impact of climate change on subsurface drainage in Iowa's subsurface drained landscapes. *Journal of Irrigation and Drainage Engineering*, *135*(4), 459–466.
Sinha, E., & Michalak, A. M. (2016). Precipitation dominates interannual variability of riverine nitrogen loading across the continental United States. *Environmental Science and Technology*, *50*(23), 12874–12884. https://doi.org/10.1021/acs.est.6b04455
Sinha, E., Michalak, A. M., & Balaji, V. (2017). Eutrophication will increase during the 21st century as a result of precipitation changes. *Science*, *357*(6349), 405–408.
Skaggs, R. W., Breve, M. A., & Gilliam, J. W. (1994). Hydrologic and water quality impacts of agricultural drainage. *Critical Reviews in Environmental Science and Technology*, *24*(1), 1–32.
Smith, S. J., & Wigley, T. M. L. (2006). Multi-gas forcing stabilization with Minicam. *Energy Journal*, *27*(Special Issue# 3), 373–391.
Thomas, P., & Rahman, M. S. (2012). Extensive reproductive disruption, ovarian masculinization and aromatase suppression in Atlantic croaker in the northern Gulf of Mexico hypoxic zone. *Proceedings of the Royal Society B: Biological Sciences*, *279*(1726), 28–38.
Thomson, A. M., Calvin, K. V., Smith, S. J., Kyle, G. P., Volke, A., Patel, P., et al. (2011). RCP4. 5: A pathway for stabilization of radiative forcing by 2100. *Climatic Change*, *109*(1), 77–94.
Tian, H., Xu, X., Liu, M., Ren, W., Zhang, C., Chen, G., & Lu, C. (2010). Spatial and temporal patterns of CH4 and N2O fluxes in terrestrial ecosystems of North America during 1979–2008: Application of a global biogeochemistry model. *Biogeosciences*, *7*(9), 2673–2694.
Tian, H., Xu, R., Pan, S., Yao, Y., Bian, Z., Cai, W., et al. (2020). Long-term trajectory of nitrogen loading and delivery from Mississippi River Basin to the Gulf of Mexico. *Global Biogeochemical Cycles*, *34*(5), e2019GB006475.
Turner, R. E., Rabalais, N. N., & Justic, D. (2006). Predicting summer hypoxia in the northern Gulf of Mexico: Riverine N, P, and Si loading. *Marine Pollution Bulletin*, *52*(2), 139–148.
Van Meter, K. J., Basu, N. B., & Van Cappellen, P. (2017). Two centuries of nitrogen dynamics: Legacy sources and sinks in the Mississippi and Susquehanna River Basins. *Global Biogeochemical Cycles*, *31*(1), 2–23. https://doi.org/10.1002/2016GB005498
Van Meter, K. J., Basu, N. B., Veenstra, J. J., & Burras, C. L. (2016). The nitrogen legacy: Emerging evidence of nitrogen accumulation in anthropogenic landscapes. *Environmental Research Letters*, *33*(3), 035014. https://doi.org/10.1088/1748-9326/11/3/035014
Van Meter, K. J., Van Cappellen, P., & Basu, N. B. (2018). Legacy nitrogen may prevent achievement of water quality goals in the Gulf of Mexico. *Science*, *360*(6387), 427–430. https://doi.org/10.1126/science.aar4462
Voldoire, A., Sanchez-Gomez, E., y Mélia, D. S., Decharme, B., Cassou, C., Sénési, S., et al. (2013). The CNRM-CM5. 1 global climate model: Description and basic evaluation. *Climate Dynamics*, *40*(9–10), 2091–2121.
Wei, Y., Liu, S., Huntzinger, D. N., Michalak, A. M., Viovy, N., Post, W. M., et al. (2014). The north American carbon program multi-scale synthesis and terrestrial model intercomparison project – Part 2: Environmental driver data. *Geoscientific Model Development*, *7*(6), 2875–2893. https://doi.org/10.5194/gmd-7-2875-2014
Westra, S., Alexander, L. V., & Zwiers, F. W. (2013). Global increasing trends in annual maximum daily precipitation. *Journal of Climate*, *26*(11), 3904–3918.
Wine, M. L., Golden, H. E., Christensen, J. R., Lane, C. R., & Makhnin, O. (2020). Seasonal watershed-scale influences on nitrogen concentrations across the Upper Mississippi River Basin. *Hydrology and Earth System Sciences Discussions*, 1–31.
Wise, M., Calvin, K., Thomson, A., Clarke, L., Bond-Lamberty, B., Sands, R., et al. (2009). Implications of limiting CO2 concentrations for land use and energy. *Science*, *324*(5931), 1183–1186.
Yang, Q., Tian, H., Li, X., Ren, W., Zhang, B., Zhang, X., & Wolf, J. (2016). Spatiotemporal patterns of livestock manure nutrient production in the conterminous United States from 1930 to 2012. *The Science of the Total Environment*, *541*, 1592–1602.
Yu, Z., & Lu, C. (2018). Historical cropland expansion and abandonment in the continental US during 1850 to 2016. *Global Ecology and Biogeography*, *27*(3), 322–333.
Yu, Z., Lu, C., Cao, P., & Tian, H. (2018). Long-term terrestrial carbon dynamics in the Midwestern United States during 1850-2015: Roles of land use and cover change and agricultural management. *Global Change Biology*, *24*(6), 2673–2690.

Yu, Z., Lu, C., Hennessy, D. A., Feng, H., & Tian, H. (2020). Impacts of tillage practices on soil carbon stocks in the US corn-soybean cropping system during 1998 to 2016. *Environmental Research Letters*, *15*(1), 14008.

Yu, Z., Lu, C., Tian, H., & Canadell, J. (2019). Largely underestimated carbon emission from land use and cover change in the conterminous U.S. *Global Change Biology*, *25*(11), 3741–3752. https://doi.org/10.1111/gcb.14768

Zhang, J., Cao, P., & Lu, C. (2021). Half-century history of crop nitrogen use efficiency budget in the conterminous United States: Variations over time, space and crop types. *Global Biogeochemical Cycles*, *35*(10), e2020GB006876. https://doi.org/10.1029/2020GB006876

Zhang, J., Felzer, B. S., & Troy, T. J. (2016). Extreme precipitation drives groundwater recharge: The Northern High Plains Aquifer, central United States, 1950–2010. *Hydrological Processes*, *30*(14), 2533–2545. https://doi.org/10.1002/hyp.10809

Zhang, J., Lu, C., Feng, H., Hennessy, D., Guan, Y., & Mba-Wright, M. (2021). Extreme climate increased crop nitrogen surplus in the United States. *Agricultural and Forest Meteorology*, *310*. https://doi.org/10.1016/j.agrformet.2021.108632

Zheng, W., Wang, S., Tan, K., & Lei, Y. (2020). Nitrate accumulation and leaching potential is controlled by land-use and extreme precipitation in a headwater catchment in the North China Plain. *The Science of the Total Environment*, *707*, 136168.